Eur. Phys. J. D **9**, 223–227 (1999)

THE EUROPEAN PHYSICAL JOURNAL D

EDP Sciences

Stability and electronic properties of pure aluminum clusters

F. Duque and A. Mañanes

Departamento de Física Moderna, Facultad de Ciencias, Universidad de Cantabria, 39005 Santander, Spain

Received: 1 September 1998 / Received in final form: 28 October 1998

Abstract. The electronic and geometrical structures of neutral and charged clusters Al_N, $N < 22$, are calculated using *ab initio* density functional theory (DFT). The geometries obtained are in agreement with those of *ab initio* molecular dynamics. The binding energy is proportional to the inverse of the cluster radius, with a slight overbinding with respect to the experiment. The vertical ionization potentials follow the oscillations found experimentally. The photoelectron density of states for the anions are in agreement with the experimental results. The s, p, and d characters of the Kohn–Sham orbitals are obtained as a function of the size, and it is shown that the s–p hybridization starts at Al_8 both for neutral and anionic clusters. The deeper Kohn–Sham eigenvalues follow the pattern of a spherical jellium-like model. The occupation of the p band is found to be one electron per atom in the cluster; this agrees with experimental results.

PACS. 36.40.Mr Spectroscopy and geometrical structure of clusters – 61.46.+w Clusters, nanoparticles

1 Introduction

There have been many experiments on the atomic clusters of s–p metallic elements, because of their technological relevance and the growing interest in (i) the size evolution of electronic properties from the atomic scale to the nanometric range and (ii) their connection with bulk properties for metals of valence greater than one [1]. For the aluminum clusters, semiclassical and simple quantal models (jellium) are able to describe the general trends of the size dependence of properties like binding energies, ionization potentials, electron affinities, and polarizabilities. However, there are deviations in the small-size region (the actual limit depends on the property) that are due to the detailed quantum behaviour of the cluster and to the interplay of the geometry with the electronic structure [1–3]. Recent experiments [4, 5] on the photoelectron spectra (PES) of anionic Al clusters with improved energy resolution give indications about the onset of the s–p hybrydization on small aluminum clusters. They have established that between Al_6^- and Al_{12}^-, there is a mixing of the uppermost antibonding $3s$-derived orbital with the $3p$ band, and that starting from Al_{13}^-, the behaviour found resembles electronic shell structure in the sense that the part of the spectrum at lower binding energy grows in intensity with increasing size of the cluster, leading to a gain of one electron per additional Al atom [5]. Furthermore, direct spectroscopic signatures, in the form of energy gaps in the PES spectra, indicate that the electronic shell closing of Al clusters are in agreement with the shell model predictions [4]. Our calculations are aimed mainly toward the understanding of these experimental facts.

2 Theoretical method

Our description is based on the self-consistent solution of the Kohn–Sham equations of DFT [6], which we use to obtain the electronic states (orbitals) for the valence electrons in the aggregate. The local density approximation (LDA) is used for the exchange-correlation energy $E_{\rm XC}[\varrho]$. The key point of the optimization of the geometrical structure is solved as follows: In a first step, the external potential on the valence electrons for a given geometry is obtained as a spherically averaged pseudopotential (SAPS) [7]. The $E_{\rm XC}$ functional used in this calculation is the one of Gunnarson and Lunqvist. In this way, the electronic states have spherical symmetry and can be labeled by the principal and angular momentum quantum numbers. Due to the spherical average, the external potential depends only on the radial coordinate of the ions in the cluster. However, the actual three-dimensional (3D) geometry of the system is taken into account in the ion–ion repulsion, and the equilibrium geometry is obtained by a simulated annealing procedure starting from initial random geometries. This approximation overemphasizes the spherical structures, even for the smallest clusters [7, 8]. As a second step, the equilibrium geometry of SAPS is used as the starting atomic configuration for a full 3D quantum chemistry calculation, also in DFT, using the Amsterdam density functional code (ADF) [9]. Next, the $E_{\rm XC}[\varrho]$ of Vosko, Wilk, and Nusair [10] is used, and the generalized gradient corrections are not included in the calculation. With the frozen core approximation for each aluminum atom (neon electronic core), the molecular orbitals for the valence electrons (three per atom) are obtained as optimized linear combinations of a basis set formed by two s, six p, and five d Slater-type atomic orbitals per atom in the aggre-

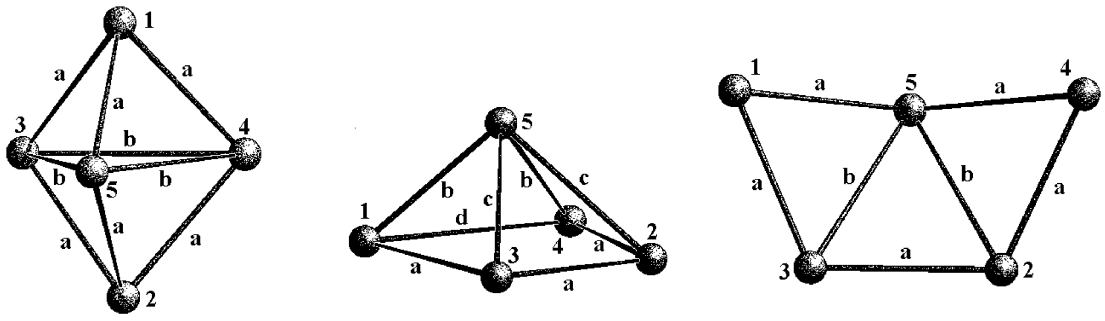

Fig. 1. Equilibrium geometries for Al_5 and Al_5^- in SAPS and ADF. The distances in angstrom are the following: Al_5(SAPS) $a = 2.53$, $b = 3.03$; Al_5(ADF) $a = 2.60$, $b = 2.48$, $c = 2.83$, $d = 3.45$; Al_5^- (ADF): $a = 2.56$, $b = 2.72$.

gate. It is relevant to note that the basis set is not orthogonal. The calculation is a spin-restricted one. However, no symmetry restrictions are imposed on the geometry, nor on the electronic states; this is so that the most general optimization and the local minimum closest to the starting geometry are reached in each calculation.

3 Results

The geometries obtained are comparable to those calculated using molecular dynamics within DFT for the small clusters [11]. An example is shown in Fig. 1 for Al_5, where the geometry of SAPS and that obtained from it in the ADF calculation are presented. The structure for Al_5^-, and in general for all the anionic clusters, is obtained starting from the corresponding neutral cluster. The method is able to substantially modify the initial structure and to obtain a nearly planar structure for the anionic case. Icosahedral structures are obtained for Al_{12} and Al_{13} in agreement with previous calculations [12].

A general description of the geometries is obtained by the analysis of the average distance to the first neighbour d_1 and the average first coordination number, n_1. The values of d_1 follow a linear behaviour in terms of $N^{-1/3}$ given by

$$\frac{d_1}{r_s z^{1/3}} = 1.779 - 0.285\, N^{-1/3}, \qquad (1)$$

where $r_s = 2.07$ a.u. is the one-electron radius of the bulk and $z = 3$ is the valence. The linear fit obtained gives approximately the right asymptotic behaviour for bulk aluminum (when $N^{-1/3} \to 0$): $d_1(\text{bulk})/r_s z^{1/3} = 1.813$. To calculate n_1, all the atoms that are closer to a given one by less than $1.3 \times d_1$ are considered. The values for n_1 are given in Fig. 2, where the line corresponds to

$$n_1 = 12.276 - 15.371\, N^{-1/3}, \qquad (2)$$

so the limit when $N^{-1/3} \to 0$ is very close to the number of nearest neighbours in bulk aluminum, $n_1(\text{bulk}) = 12$. The linear behaviour of d_1 and n_1 gives an indication of how the clusters grow: There is a very slight increase of the distance to the nearest neighbours as the size N increases, while the number of neighbours n_1 grows quickly as the number of atoms in the aggregate increase.

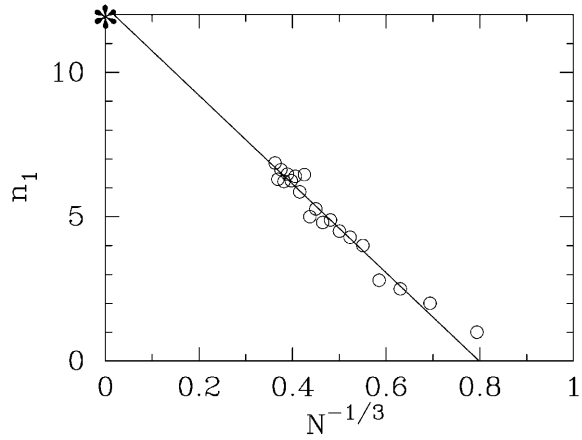

Fig. 2. Average values of the first coordination number, n_1, as a function of $N^{-1/3}$. The line follows the fit described in the text. The bulk value for n_1 is 12.

The binding energy per atom for neutral clusters is presented in Fig. 3 as a function of the inverse of the cluster size, $N^{-1/3}$, and compared with the experimental results. A systematic overbinding of less than 0.5 eV/atom is obtained, but both the increased stability of Al_{13} with respect to Al_{12} and the linear dependence on $N^{-1/3}$ are well reproduced by the present results. The size dependence of the vertical ionization potential and its comparison with experiments are also given in Fig. 3. In this case, several facts are well reproduced: the increment with respect to the atomic value for the smaller clusters, the drops at $N = 5$ and at $N = 7$ (the last one is linked with the transition from 18 electrons, or two less than the "magic number" 20, to 21, or one more than the "magic number"), the behaviour around $N = 13$ (one electron less than the spherical "magic number" 40), and the nearly perfect reproduction of the even–odd effect in the region $N = 14$ to $N = 21$ (with the exception of $N = 20$). Our results of Fig. 3 are also comparable with very recent calculations [13].

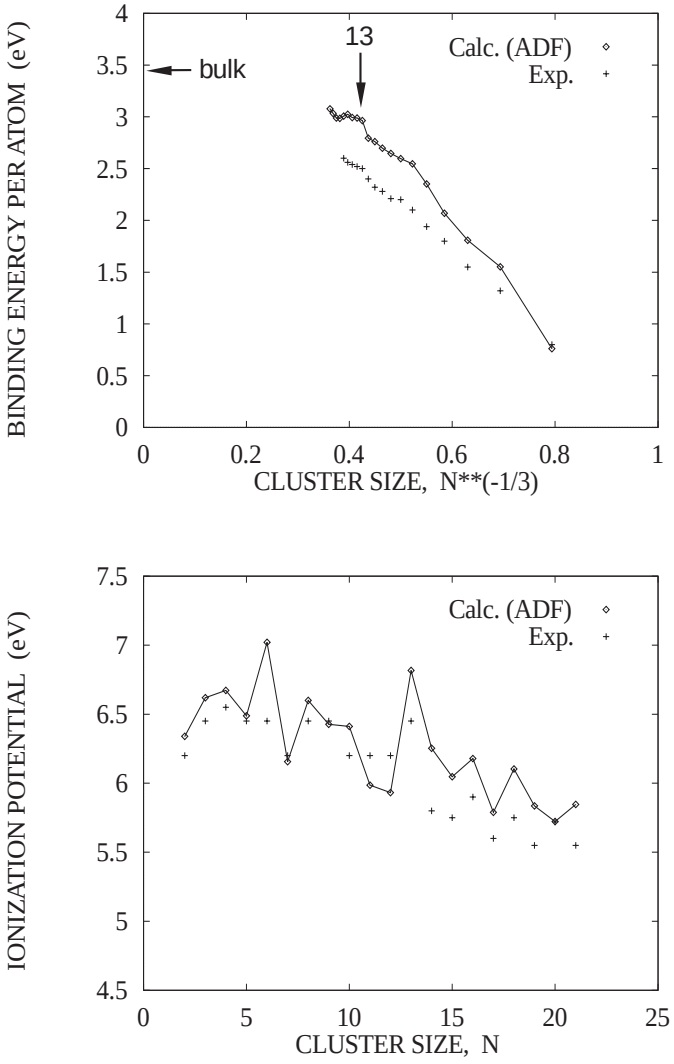

Fig. 3. Binding energies and vertical ionization potentials.

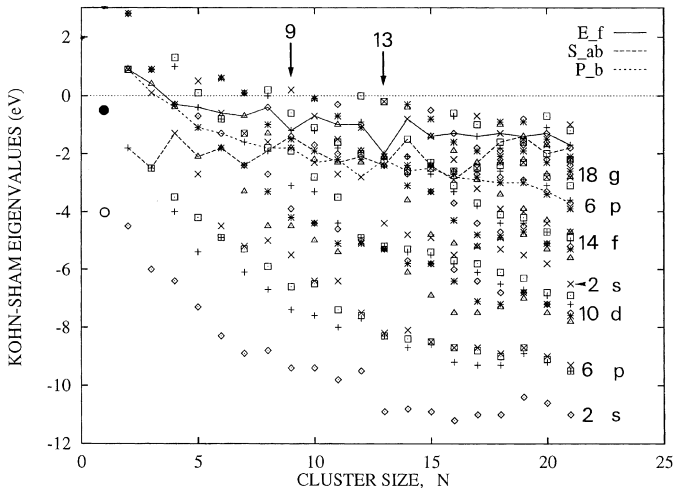

Fig. 4. Kohn–Sham eigenvalues for Al_N^-. The lines indicate the Fermi level (E_f), the $3s$ antibonding state (S_{ab}) and the $3p$ bonding state (P_b). The labels on the right give the degeneracy and the angular momentum on a spherical model. For $N = 1$, the symbols indicate the experimental values for Al^-.

The single-particle Kohn–Sham eigenvalues for Al_N^- are given in Fig. 4. They can be considered as an estimation of the electronic density of states for these clusters; the figure gives their size evolution. Three lines are indicated in Fig. 4. The first one gives the Fermi level, E_f. The comparison with experiments [5] indicates that our result is shifted to lower binding energies by 2.5 eV for $N = 2$ and by 1.5 eV for the largest cluster $N = 21$. This effect may be related to the wrong long-distance behaviour of the exchange-correlation potential in the LDA. The second line, S_{ab}, links the states of highest energy for which the s character is dominant. These states should correspond with the s-antibonding state described in [5]. The third line, P_b, links the states of lowest energy for which the p characater is dominant. These states should correspond with the lower limit of the p band in the bulk, and the region between these states and the Fermi level is the occupied part of the p band. This region has an analogous shape to that described in the experiments (Fig. 3 of [5]), and the narrowing of the p band at $N = 9$ and $N = 13$ is in agreement with those experimental results. Another remarkable result from the figure is that $N = 8$ is the first cluster for which the s-antibonding state is mixed with the p band, in agreement with the experiments [4, 5]. This mixing can be related to the increment in the number of first neighbours described in Fig. 2. Finally, the right-hand side of Fig. 4 indicates the labeling of the eigenvalues according to the electronic spherical shells, given the occupation and the corresponding angular momentum. We remind the reader that, due to the lack of symmetry, any single-particle state in our calculation has only a degeneracy of two. From the results we can see that, for the biggest clusters, the standard order for the electronic levels in a spherical external potential (jellium or SAPS models) is recovered, and that the degeneracy is only partially removed for the internal shells. The agreement with the spherical model is not only qualitative but also quantitative, in the case of neutral clusters, as far as the eigenvalues obtained in the SAPS calculation give an accurate average of those obtained in the ADF method. When the characters s, p, and d of each single-particle state are obtained, the corresponding s, p, and d character of the Slater orbitals of the basis set are taken into account. In spite of the nonorthogonality of the basis, only the diagonal contributions to s, p, and d are considered when the corresponding character is obtained.

In order to compare with the measured PES [4, 5] we have constructed the electronic densities of states starting from the calculated Kohn–Sham eigenvalues and folding them with a Lorentzian function, the width of which, 300 meV, is given by the resolution of the experiments (100–300 meV) [5]. The results for two selected clusters are given in Fig. 5. The s, p, and d contributions are also indicated, and only the occupied states are presented in the plots. Only the anions can be compared with the experiments [4, 5] and the agreement is quite good, in spite of the general shift to higher energies (less binding) obtained in our calculation. For Al_{13}^- there is a single peak with

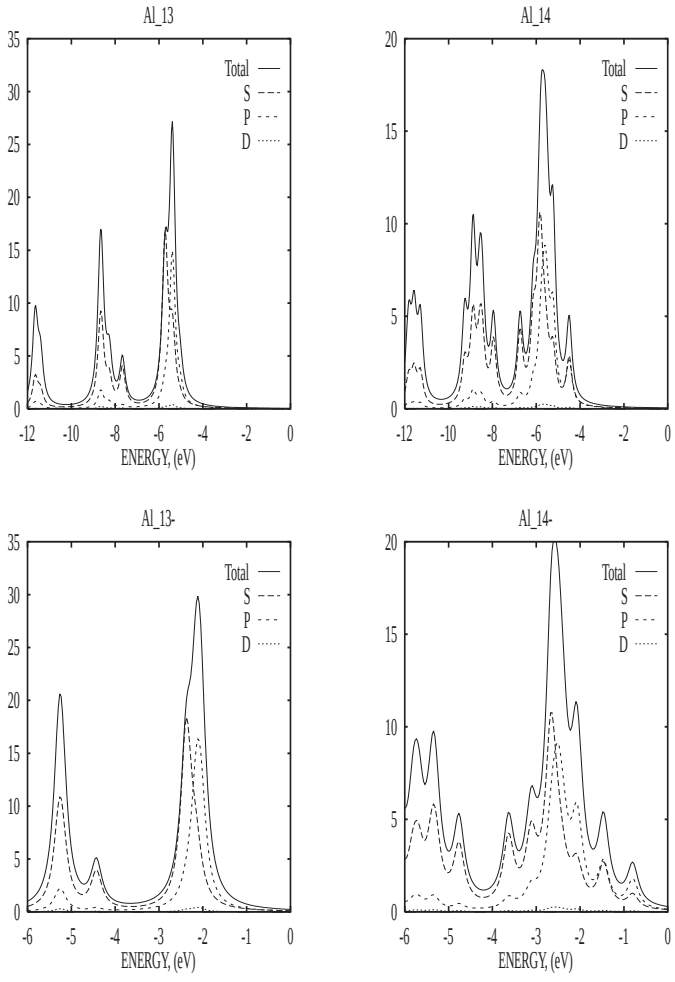

Fig. 5. Electronic density of states for neutral and anionic clusters with the s, p, and d partial contributions.

a left shoulder which, according to our results, is due to a dominant s state below the Fermi level, which is of p character. For Al_{14}^-, the two picks of dominant p character that appear at the right of the main one (also of p character) are in agreement with those found experimentally. Our conclusion is that the comparisson between the calculated and measured high-resolution PES can be used as a fine tool for the elucidation of the geometry of the aggregates, as has been pointed out elsewhere [14]. The general shift of the single-particle states to higher energies obtained in our calculation for the anionic clusters must be due to the wrong exponential decay of the LDA exchange-correlation part of the effective potentials. For neutral clusters, the right asymptotic behaviour is $-1/r$, and for the negatively charged systems, this drawback has even more influence. A better way to perform the comparisons with the experiments might be to displace the Fermi level of the anions to the calculated value of the electron affinity.

Once the lower limit of the p band is defined as the state with the lowest energy in the collection of those with dominant p character (this limit is the line P_b on Fig. 4), the population of the band is obtained by the summing up of occupations up to the Fermi level. The results are presented in Fig. 6 for anionic clusters. The trend obtained is in agreement with the electronic shell picture supported by the experiments [5]: There is an increment of one electron in the p band per additional Al atom in the cluster, so the other two valence electrons are located in deeper states. The strong deviation for $N = 12$ is due to the high degeneracy of the electronic states of a cluster with icosahedral symmetry.

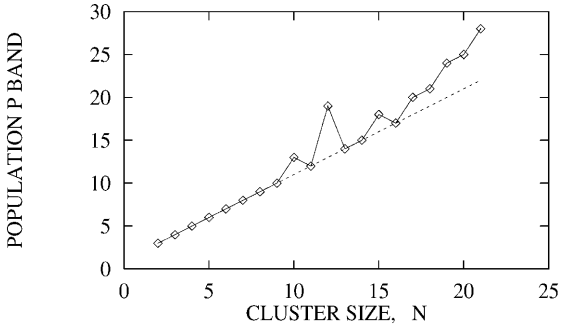

Fig. 6. Size evolution of the occupation of the p band for Al_N^- clusters. The dashed line corresponds to one electron per atom.

4 Conclusions

The method proposed gives a good description of the properties of s–p metallic clusters, including photoelectron spectra of the anions. It is able to describe the band formation in these clusters, and to establish that for aluminum, the s–p hybridizations start at Al_8, because of the increment in the number of first neighbours. It is possible to define a p band in these clusters, and the calculation shows that its occupation increments in one electron per additional Al atom in the cluster. The actual geometries of the clusters remove the spherical degeneracy of the electronic states; however, some memory of the spherical character remains for the deeper states of the large clusters. Finally, the geometries obtained with simplified models (SAPS) are a good starting point for more fundamental quantum chemistry calculations.

We thank J.A. Alonso, J.A. Aramburu, M.T. Barriuso, M.P. Iñiguez, and M. Moreno for their suggestions, and the Spanish CICYT, PB95–0581, for financial support.

References

1. M.F. Jarrold: in *Clusters of Atoms and Molecules I*, ed. by H. Haberland (Springer, Berlin 1995) p. 288
2. W. de Heer: Rev. Mod. Phys. **65**, 611 (1993)
3. M. Brack: Rev. Mod. Phys. **65**, 677 (1993)
4. X. Li, H. Wu, X.B. Wang, L.S. Wang: Phys. Rev. Lett. **81**, 1909 (1998)

5. G. Ganteför, W. Eberhardt: Chem. Phys. Lett. **217**, 600 (1994); C.-Y. Cha, G. Ganteför, W. Eberhardt: J. Chem. Phys. **100**, 995 (1994)
6. W. Kohn: in *Density Functional Theory*, ed. by E.K.U. Gross, R.M. Dreizler (Plenum Press, New York 1995)
7. M.P. Iñiguez, M.J. López, J.A. Alonso, J.M. Sóler: Z. Phys. D **11**, 163 (1989)
8. J.G. Aguilar, A. Mañanes, M.J. López, M.P. Iñiguez, J.A. Alonso: Int. J. Quantum Chem. **56**, 589 (1995); A. Mañanes, M.P. Iñiguez, M.J. López, J.A. Alonso: Phys. Rev. B **42**, 5000 (1990)
9. G. te Velde, E.J. Baerends: J. Comput. Chem. **99**, 84 (1992); P.M. Boerriger, G. te Velde, E.J. Baeredens: Int. J. Quantum Chem. **33**, 87 (1988)
10. S.H. Vosko, L. Wilk, M. Nusair: Can. J. Phys. **58**, 1200 (1980)
11. P. Calaminici, N. Russo, M. Toscano: Z. Phys. D **33**, 281 (1995); R.O. Jones: J. Chem. Phys. **99**, 1194 (1993)
12. J.E. Fowler, J.M. Ugalde: Phys. Rev. A **58**, 383 (1998); S.H. Yang, D.A. Drabold, J.B. Adams, A. Sachdev: Phys. Rev. B **47**, 1567 (1993); H.-P. Cheng, R.S. Berry, R.L. Whetten: Phys. Rev. B **43**, 10 647 (1991)
13. J. Akola, H. Häkkinen, M. Manninen: Phys. Rev. B **58**, 3601 (1998)
14. H. Handschuh, G. Ganteför, W. Eberhardt: Rev. Sci. Instrum. **66**, 3838 (1995)